13-atom metallic clusters studied by density functional theory: Dependence on exchange-correlation approximations and pseudopotentials

J. P. Chou,[1,2] H. Y. T. Chen,[1,3] C. R. Hsing,[1] C. M. Chang,[4] C. Cheng,[5] and C. M. Wei[1,6,*]
[1]*Institute of Atomic and Molecular Sciences, Academia Sinica, Taipei 106, Taiwan*
[2]*Department of Physics, National Chung Cheng University, Chia-Yi 621, Taiwan*
[3]*Department of Chemistry, University College London, London WC1H 0AJ, United Kingdom*
[4]*Department of Physics, National Dong Hwa University, Hualien 974, Taiwan*
[5]*Department of Physics, National Cheng Kung University, Tainan 701, Taiwan*
[6]*Institute of Physics, Academia Sinica, Nankang, Taipei 115, Taiwan*
(Received 8 July 2009; revised manuscript received 18 September 2009; published 16 October 2009)

In this study, the 13-atom cluster structures of alkaline metals, alkaline-earth metals, boron group metals, carbon group metals, and 3*d*, 4*d*, and 5*d* transition metals in the periodic table are investigated by density functional theory with three kinds of exchange-correlation (XC) functionals: (i) local-density approximation (LDA); (ii) generalized gradient approximation (GGA) with Perdew-Wang 91; and (iii) generalized gradient approximation with Perdew-Burke-Ernzerhof. The dependence on pseudopotentials (PPs) with and without semicore electrons is also examined. The relative energies of five selected high-symmetry three-dimensional and four low-symmetry layer-type isomers for each element of interest are calculated and studied. Among the 44 metallic 13-atom clusters, our results show that the two GGA XC functionals have a great consistency; LDA and GGA results also reveal a great consistency, apart from the Cr, Mn, Fe, Co, Ni, and Rh 13-atom clusters, for which the results show a significant difference. Meanwhile, for most of the elements, the calculations with and without semicore PPs also produce consistent results, except for Cr, Mo, and V, which require a careful treatment of semicore states in the PPs.

DOI: 10.1103/PhysRevB.80.165412 PACS number(s): 31.15.E−, 36.40.−c, 61.46.Bc

I. INTRODUCTION

Metallic clusters play crucial roles in a wide range of nanotechnology applications,[1] such as catalysis, electronics, magnetics, and optics,[2,3] due to their novel physical and chemical properties that vary with cluster size, geometric structure, and temperature.[4,5] To probe and understand the properties of these metallic clusters, the first step is to investigate their lowest-energy structures. The most studied aggregates are 13-atom clusters because they correspond to the first geometric shell closing for all icosahedral, decahedral, and cuboctahedral structures. Sakurai *et al.*[6] experimentally showed that 13 is a common magic number for many transition-metal clusters including Fe_{13}, Ti_{13}, Zr_{13}, Nb_{13}, and Ta_{13} but could not provide clear evidence for the exact atomic arrangement. Until now, it has been difficult and rare to directly probe the structures of such small clusters experimentally.

Theoretically, 13-atom metallic clusters have been intensively studied[7–14] via density functional theory (DFT) (Ref. 15) in the past decade. Nevertheless, some controversy and uncertainty concerning the ground-state structure of 13-atom clusters are found in the literature. For instance, by using high-resolution photoelectron spectroscopy and density functional calculations, Häkkinen *et al.*[16] found that small Au clusters (fewer than 13 atoms) prefer a two-dimensional layered structure, due to strong relativistic effects. However, Oviedo *et al.*[17] found that Cu_{13}, Ag_{13}, and Au_{13} prefer a disordered or amorphous ground structure. On the other hand, the determination of the global minima of a cluster is not a trivial issue. Kumar *et al.*[18,19] found that Ru, Rh, and Pd clusters from 13, 55, to 147 atoms show icosahedral growth by spin-polarized DFT-generalized gradient approximation (GGA) calculations. However, Bae *et al.*[20] found that the Rh_{13} cluster strongly prefers a cage structure with a magnetic moment of $17\mu_B$, which is 0.30 eV lower than that of the icosahedral structure with the magnetic moment of $21\mu_B$. Furthermore, Wang *et al.*[11] also reported that 4*d* and 5*d* late transition metals with open *d* orbitals such as Rh_{13}, Pt_{13}, and Pd_{13} prefer low-symmetry open structures rather than high-symmetry compact structures. As one can see from the above results[18–20] for Rh_{13} cluster, even using DFT with the same exchange-correlation (XC) functional (GGA) to find the global minimum structure for a specific element and cluster size, different results and conclusions might be obtained due to an incomplete search in multidimensional space. There is another issue that must be clarified. The relative energies for various isomers of the same metallic cluster obtained by using different XC functionals may not give the same energy ordering, as commonly believed. Therefore, regarding the relative energies of metallic isomers, a systematical study for their dependence on various XC functionals is inevitable and necessary. Some preliminary studies following this direction can be found in the literature.[12,21]

The commonly used XC functionals, in the DFT approach with pseudopotential (PP) approximation, are local-density approximation (LDA),[22] Perdew-Wang 91 (PW91),[23] and Perdew-Burke-Ernzerhof (PBE).[24] DFT-GGA (PW91 and PBE) has been shown to be very effective for bulk and surface calculations. Nonetheless, for metallic cluster systems, the consistency of various XC functionals used in calculations has not been seriously studied. Furthermore, despite the success of PP approximations,[25] the necessity of semicore usage has not been deliberately examined. Hence, a guide-

line of how to choose a feasible XC functional and suitable PPs to obtain robust and reliable results is of significance. The focal point of this work is a systematic study of the dependence of various XC functionals including LDA, PW91, and PBE, as well as the influence of semicore states, on the relative stability of nine isomers applied on 44 metals throughout the periodic table. To compare and verify the validity of different XC functionals and PPs, we calculate the relative energies by spin-polarized DFT and introduce a correlation analysis to provide quantitative comparisons of the results between different XC functionals and/or PPs. Our results strongly suggest that in the study of 13-atom metallic clusters, DFT calculations using different XC functionals or PPs exhibit a great consistency and are thus reliable, except for the following two situations: (1) for Cr, Mn, Fe, Co, Ni, and Rh, the results show that LDA and GGA have a great inconsistency (GGA is more reliable, as expected); (2) PPs with and without semicore states for Cr, Mo, and V produce contradictory results, and thus for Cr, Mo, and V, cautious usage of PPs is strongly recommended.

This paper is organized as follows. The computational details are given in Sec. II. The calculated relative isomer energies for 13-atom metallic clusters, including their dependences on various XC functionals and PPs, are presented and discussed in Sec. III. The summary and conclusion are presented in Sec. IV.

II. COMPUTATIONAL DETAILS

The 13-atom metallic cluster structures of the alkaline metals (IA), alkaline-earth metals (IIA), boron group metals (IIIA), and carbon group metals (IVA), 3*d*, 4*d*, and 5*d* transition metals in the periodic table are investigated by spin-polarized DFT with three kinds of XC approximations: (i) LDA, (ii) PW91, and (iii) PBE. The calculations are carried out with the Vienna *ab initio* simulation package (VASP) (Ref. 26) and its corresponding PP database. The Kohn-Sham orbitals are expanded in a plane-wave basis set and the interactions of the valence electrons with the ionic cores are described by the projected augmented wave (PAW) (Ref. 27) potentials. The kinetic-energy cutoffs used are the maximal default values recommended by the VASP (Ref. 26) PP database, which range from 81.4 (sodium) to 700.0 (sodium with the *s-type* semicore state) eV. A unit cell size of $20\times20\times20$ or $24\times24\times24$ Å^3, depending upon the cluster size, is used to prevent interactions between neighboring unit cells. Due to the large unit cell size, only the gamma point is used to sample the Brillouin zone integration. For the optimized geometries, the convergence criterion is 10^{-5} eV for the self-consistent electronic loop and the force on each atom is less than 0.03 eV/Å.

There are many isomers that are energetically favorable for clusters with 13 atoms. In this work, we do not intend to find the global minimum isomer structure. Instead, our focus point is to systematically study the dependence of the relative stability of metallic cluster isomers by using different XC functionals and/or semicore state PPs. To achieve this purpose, we have selected and constituted a sampling set with nine different and representative structures to study, as shown in Fig. 1. For three-dimensional structures, we chose five well-known high-symmetry structures as follows: icosahedral (ICO) with I_h symmetry, cuboctahedral (FCC) with O_h symmetry, decahedral (DEC) with D_{5h} symmetry, body-centered cubic (BCC) with D_{4h} symmetry, and hexagonal close packed (HCP) with D_{3d} symmetry. For two-dimensional structures, four layer-type structures are considered: buckled biplanar (BBP) (Ref. 7) with C_{2v} symmetry, triangular biplanar (TBP) (Ref. 9) with C_{3v} symmetry, garrison-cap layer (GCL) with C_{2v} symmetry, and cagelike (CAG) (Ref. 28) structures with C_{1h} symmetry. For a particular isomer structure, a significant distortion may occur, for example, Nb 13-atom clusters.[29] However, in this work, we maintain the cluster symmetry as mentioned above.

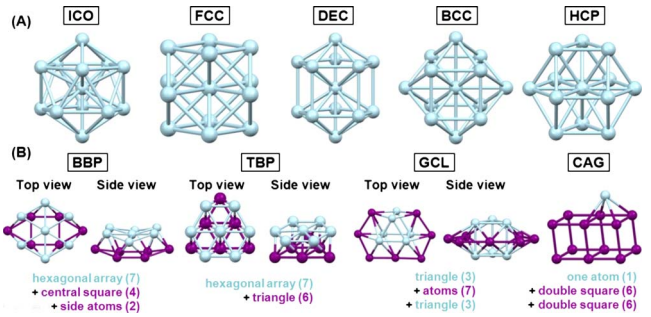

FIG. 1. (Color online) Nine isomer structures of 13-atom clusters. (a) Five high-symmetry three-dimensional structures; (b) four low-symmetry layer-type structures.

III. RESULTS AND DISCUSSION

The relative energies of nine isomer structures of 13-atom metallic clusters throughout the periodic table have been investigated systematically by using three XC functionals (LDA, PW91, and PBE) and their corresponding PPs with or without semicore states. For the purpose of making a quantitative and elaborate comparison of the relative energies using different XC functionals and PPs, we introduce an n-dimensional displacement vector, $\vec{\mathfrak{D}}=(r_1,r_2,\ldots,r_n)$, where n represents the total number of the structural isomers (here, $n=9$) and r_i is the relative energy defined as $r_i=E_i-\bar{E}$, where E_i and $\bar{E}$ are the total energy of a certain isomer and the average energy of all the isomers, respectively. In this study, we define the displacement vectors as $\vec{\mathfrak{D}}^A_{M(a)}$ and $\vec{\mathfrak{D}}^B_{M(b)}$, where A and B represent either LDA, PW91 and PBE; M represents the selected metal element; and a and b represent the semicore states of PPs (including *s*-type, *p*-type, or *d*-type orbitals, denoted as *sv*, *pv*, and *d*, respectively), and the subscript is ignored for PPs without the semicore state. The correlation between $\vec{\mathfrak{D}}^A_{M(a)}$ and $\vec{\mathfrak{D}}^B_{M(b)}$ vectors can be determined from their inner product ($\cos\boldsymbol{\theta}$) and relative amplitude ($\boldsymbol{L}$) as follows:[30]

$$\cos(\boldsymbol{\theta})=\frac{\vec{\mathfrak{D}}^A_{M(a)}\cdot\vec{\mathfrak{D}}^B_{M(b)}}{(|\vec{\mathfrak{D}}^A_{M(a)}||\vec{\mathfrak{D}}^B_{M(b)}|)}, \tag{1}$$

and

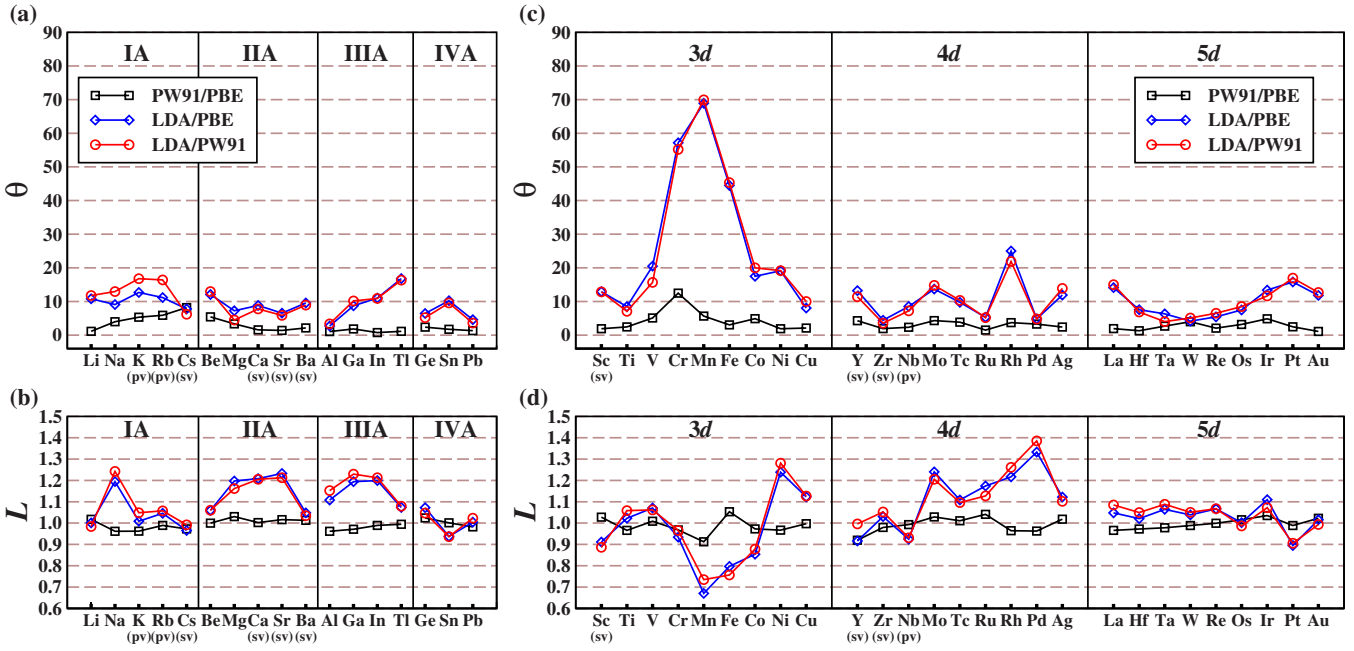

FIG. 2. (Color online) The correlation data between different XC functionals of 13-atom metallic cluster of 44 elements via periodic table. The results of angle $\boldsymbol{\theta}$ and the relative amplitude $\boldsymbol{L}$, defined in Eqs. (1) and (2), are summarized in (a) and (b) for Group A and (c) and (d) for Group B. The black square, blue diamond, and red circle represent the comparative results of two XC functionals A/B are PW91/PBE, LDA/PBE, and LDA/PW91, respectively.

$$\boldsymbol{L} = \frac{|\vec{\mathfrak{D}}^{A}_{M(a)}|}{|\vec{\mathfrak{D}}^{B}_{M(b)}|}. \tag{2}$$

If the cosine value is equal to 1 (angle $\boldsymbol{\theta}$ is equal to 0) and the relative amplitude is equal to 1, then $\vec{\mathfrak{D}}^{A}_{M(a)}=\vec{\mathfrak{D}}^{B}_{M(b)}$, which indicates that $\vec{\mathfrak{D}}^{A}_{M(a)}$ and $\vec{\mathfrak{D}}^{B}_{M(b)}$ are identical and the two calculated results are exactly the same. The correlation analyses between the displacement vectors defined above can be used to quantitatively analyze and measure the consistency of calculated results using different XC functionals and/or PPs.

In Secs. III A and III B, we use a correlation analysis as defined in Eqs. (1) and (2) to study the dependence of the relative stability of isomer structures throughout the periodic table with different XC functionals and PPs. Group A (IA, IIA, IIIA, and IVA groups) and Group B (3*d*, 4*d*, and 5*d* transition metals) are separately discussed in Secs. III A and III B. In Sec. III C, the relative deviation between two displacement vectors, combined with the results of $\boldsymbol{L}$ and $\cos(\boldsymbol{\theta})$, is introduced.

A. Group A: IA, IIA, IIIA, and IVA groups

1. Exchange-correlation dependence

In Sec. III A 1, the correlations between (1) LDA and PW91 (denoted as $\vec{\mathfrak{D}}^{\mathrm{LDA}}_{M}/\vec{\mathfrak{D}}^{\mathrm{PW91}}_{M}$), (2) LDA and PBE (denoted as $\vec{\mathfrak{D}}^{\mathrm{LDA}}_{M}/\vec{\mathfrak{D}}^{\mathrm{PBE}}_{M}$), and (3) PW91 and PBE (denoted as $\vec{\mathfrak{D}}^{\mathrm{PW91}}_{M}/\vec{\mathfrak{D}}^{\mathrm{PBE}}_{M}$) for the selected elements in Group A are investigated. Their angle $\boldsymbol{\theta}$ and the relative amplitude $\boldsymbol{L}$ are shown in Figs. 2(a) and 2(b). All PPs used in this section are without the semicore states, except for K(pv), Rb(pv), Cs(sv), Ca(sv), Sr(sv), and Ba(sv), where PPs without the semicore state are not available. Figures 2(a) and 2(b) reveal that the correlation data from two types of GGA ($\vec{\mathfrak{D}}^{\mathrm{PW91}}_{M}/\vec{\mathfrak{D}}^{\mathrm{PBE}}_{M}$, depicted as black squares) exhibit a remarkable similarity. The angle $\boldsymbol{\theta}$ values between PW91 and PBE are all smaller than 6°, except for the angle of Cs_{13}, which is 8.2°; furthermore, their relative amplitudes are all within 1.00 ± 0.05, which indicates that the results obtained from PW91 and PBE are distinctly correspondent. The consistency between LDA and GGA is also observed for most elements, which is demonstrated in Figs. 2(a) and 2(b) (red circles for $\vec{\mathfrak{D}}^{\mathrm{LDA}}_{M}/\vec{\mathfrak{D}}^{\mathrm{PW91}}_{M}$ and blue diamonds for $\vec{\mathfrak{D}}^{\mathrm{LDA}}_{M}/\vec{\mathfrak{D}}^{\mathrm{PBE}}_{M}$). The angle $\boldsymbol{\theta}$ values of the elements in Group A are smaller than 12°, except for K(pv), Rb(pv), and Tl, whose angles are roughly 17°. To more clearly present the results of Figs. 2(a) and 2(b), a few examples illustrating the agreement between different XC functionals are given in the following.

For the results of Al_{13} and Pb_{13}, the angles $\boldsymbol{\theta}$ values of $\vec{\mathfrak{D}}^{\mathrm{LDA}}_{M}/\vec{\mathfrak{D}}^{\mathrm{PW91}}_{M}$, $\vec{\mathfrak{D}}^{\mathrm{LDA}}_{M}/\vec{\mathfrak{D}}^{\mathrm{PBE}}_{M}$, and $\vec{\mathfrak{D}}^{\mathrm{PW91}}_{M}/\vec{\mathfrak{D}}^{\mathrm{PBE}}_{M}$ are all smaller than 5°. Meanwhile, the $\boldsymbol{L}$ values are within 1.00 ± 0.16. This is regarded as an impressive agreement, which can be verified by the relative energy profiles displayed in Figs. 3(a) and 3(b). Notably, the relative energies of the Al_{13} and Pb_{13} isomers calculated by these three XC functionals are well matched and consistent.

To view and analyze the quality of agreement for a larger angle $\boldsymbol{\theta}$, the relative energy profiles of $K_{13}(pv)$, $Rb_{13}(pv)$, and Tl_{13} clusters are presented in Figs. 3(c)–3(e). For $K_{13}(pv)$ and $Rb_{13}(pv)$, Fig. 2(a) shows that the angle $\boldsymbol{\theta}$ values of $\vec{\mathfrak{D}}^{\mathrm{LDA}}_{\mathrm{K}(pv)}/\vec{\mathfrak{D}}^{\mathrm{PW91}}_{\mathrm{K}(pv)}$ and $\vec{\mathfrak{D}}^{\mathrm{LDA}}_{\mathrm{Rb}(pv)}/\vec{\mathfrak{D}}^{\mathrm{PW91}}_{\mathrm{Rb}(pv)}$ are 17° and 15°, respectively. As shown in the relative energy profiles of Figs. 3(c) and 3(d), the results from LDA have a larger deviation

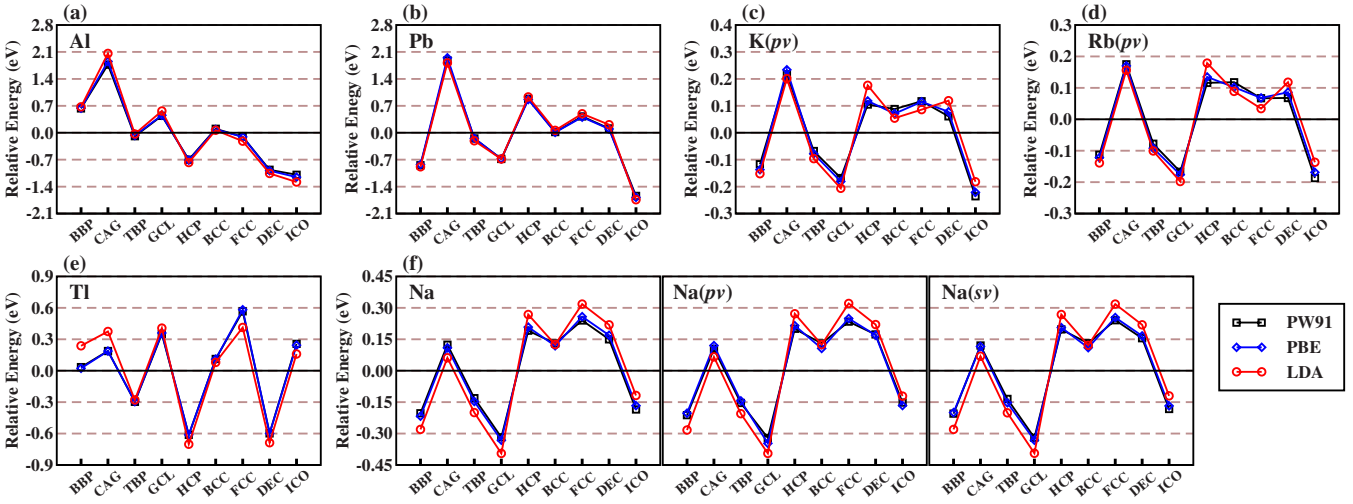

FIG. 3. (Color online) Relative energy plots of 13-atom clusters of (a) Al; (b) Pb; (c) K(pv); (d) Rb(pv); (e) Tl; (f) Na, Na(pv), and Na(sv), which are obtained from XC functionals of PW91 (black square), PBE (blue diamond), and LDA (red circle).

in the HCP, FCC, and ICO isomer structures. However, the energy difference of two degenerate minima between the GCL and ICO isomer structures obtained from LDA or GGA is smaller than 80 meV. Therefore, the prediction of the local minimum structure among the nine isomers from LDA and GGA is consistent. As for Tl_{13}, the angle $\boldsymbol{\theta}$ values of $\vec{\mathfrak{D}}_{Tl}^{LDA}/\vec{\mathfrak{D}}_{Tl}^{PW91}$ and $\vec{\mathfrak{D}}_{Tl}^{LDA}/\vec{\mathfrak{D}}_{Tl}^{PBE}$ are 16°. In Fig. 3(e), an increased relative energy for BBP and CAG and a decreased relative energy for FCC can be observed.

As a whole, in the study of metallic clusters in Group A, despite a small deviation in the relative energy for one or two isomers in some elements, the calculated results from LDA and GGA are consistent and reliable. Examining all of the studies, the results demonstrate that the value of the angle $\boldsymbol{\theta}$ is dependent on the deviation of the relative energy; in particular, when the various XC functionals result in a different energy ordering, a larger value of angle $\boldsymbol{\theta}$ might be expected.

2. Pseudopotential dependence

The correlation results between different PPs with and without considering semicore states for the IA–IVA groups are illustrated in Figs. 4(a) and 4(b). The PPs with semicore states available from the VASP (Ref. 26) database include 13 elements: Li, Na, K, Rb, Be, Mg, Ca, Ga, In, Tl, Ge, Sn, and Pb. For the study of PP dependence, there exist five combinations as follows: (i) $\vec{\mathfrak{D}}_{M}^{XC}/\vec{\mathfrak{D}}_{M(pv)}^{XC}$ for M=Mg; (ii) $\vec{\mathfrak{D}}_{M}^{XC}/\vec{\mathfrak{D}}_{M(sv)}^{XC}$ for M=Li and Be; (iii) $\vec{\mathfrak{D}}_{M(pv)}^{XC}/\vec{\mathfrak{D}}_{M(sv)}^{XC}$ for M=K, Rb, and Ca; (iv) $\vec{\mathfrak{D}}_{M}^{XC}/\vec{\mathfrak{D}}_{M(pv)}^{XC}$, $\vec{\mathfrak{D}}_{M}^{XC}/\vec{\mathfrak{D}}_{M(sv)}^{XC}$, and $\vec{\mathfrak{D}}_{M(pv)}^{XC}/\vec{\mathfrak{D}}_{M(sv)}^{XC}$ for M=Na; (v) $\vec{\mathfrak{D}}_{M}^{XC}/\vec{\mathfrak{D}}_{M(d)}^{XC}$ for M=Ga, In, Tl, Ge, Sn, and Pb. For instance, in the VASP (Ref. 26) database, Na has three types of PPs [Na, Na(pv), and Na(sv)]; thus, we can have three comparisons between three displacement vectors, $\vec{\mathfrak{D}}_{Na}^{XC}$, $\vec{\mathfrak{D}}_{Na(pv)}^{XC}$, and $\vec{\mathfrak{D}}_{Na(sv)}^{XC}$.

Employing three types of PPs for Na, we can obtain a more complete perspective for understanding the necessity of using the semicore states. Substantially, Na, Na(pv), and Na(sv) treat the $3s^1$, $2p^6 3s^1$, and $2s^2 2p^6 3s^1$ states as valence states, respectively. For Na_{13} in Fig. 4(a), the angle $\boldsymbol{\theta}$ values of $\vec{\mathfrak{D}}_{Na}^{XC}/\vec{\mathfrak{D}}_{Na(pv)}^{XC}$, $\vec{\mathfrak{D}}_{Na}^{XC}/\vec{\mathfrak{D}}_{Na(sv)}^{XC}$, and $\vec{\mathfrak{D}}_{Na(pv)}^{XC}/\vec{\mathfrak{D}}_{Na(sv)}^{XC}$ are all below 6°, and the $\boldsymbol{L}$ values range from 0.99 to 1.01. Considering the corresponding relative energy profiles in Fig. 3(f), we find that the relative energy curves of Na, Na(pv), and Na(sv) with three XC functionals exhibit high similarity, which indicates that the PP with the semicore states is not necessary. For the other 12 elements, as mentioned above, Figs. 4(a) and 4(b) show that most of the angles $\boldsymbol{\theta}$ values are below 6° and the $\boldsymbol{L}$ values are in the range from 0.98 to 1.03. Hence, the usage of semicore PPs for these elements is also unnecessary. It is concluded that the calculation results of 13-atom metallic clusters in Group A carried out without semicore PPs will lead to reliable results.

The magnetic moments of nine isomer structures of 13-atom metallic clusters for IA–IVA group elements are given in Table I. The magnetic moments are determined by setting from an initial value and then use fixed moment method to scan the moment dimension. It is found that all the magnetic moments obtained by using PW91 is essentially equal to that by PBE, except for TBP and CAG structures of Cs_{13}(sv). In most case, the moment calculated by using LDA is also equal to that of GGA, except for FCC of Ba_{13}(sv), BCC of Mg_{13}(pv), HCP of Ba_{13}(sv), GCL of Ca_{13}(sv) and Sr_{13}(sv) where the magnetic moments obtained from LDA and GGA only differ by $2\mu_B$.

B. Group B: 3*d*, 4*d*, and 5*d* transition metals

1. Exchange-correlation dependence

In Sec. III B 1, the correlation analyses between different XC functionals for 13-atom clusters of 3d, 4d, and 5d transition metals are provided, and the results are shown in Figs. 2(c) and 2(d). Most of the PPs applied here do not consider the semicore states, except for Sc(sv), Y(sv), Zr(sv), and Nb(pv).

In Figs. 2(c) and 2(d), correlation results reveal that the relative energies from PW91 and PBE (depicted as black squares) have a high correspondence with all of the angle $\boldsymbol{\theta}$

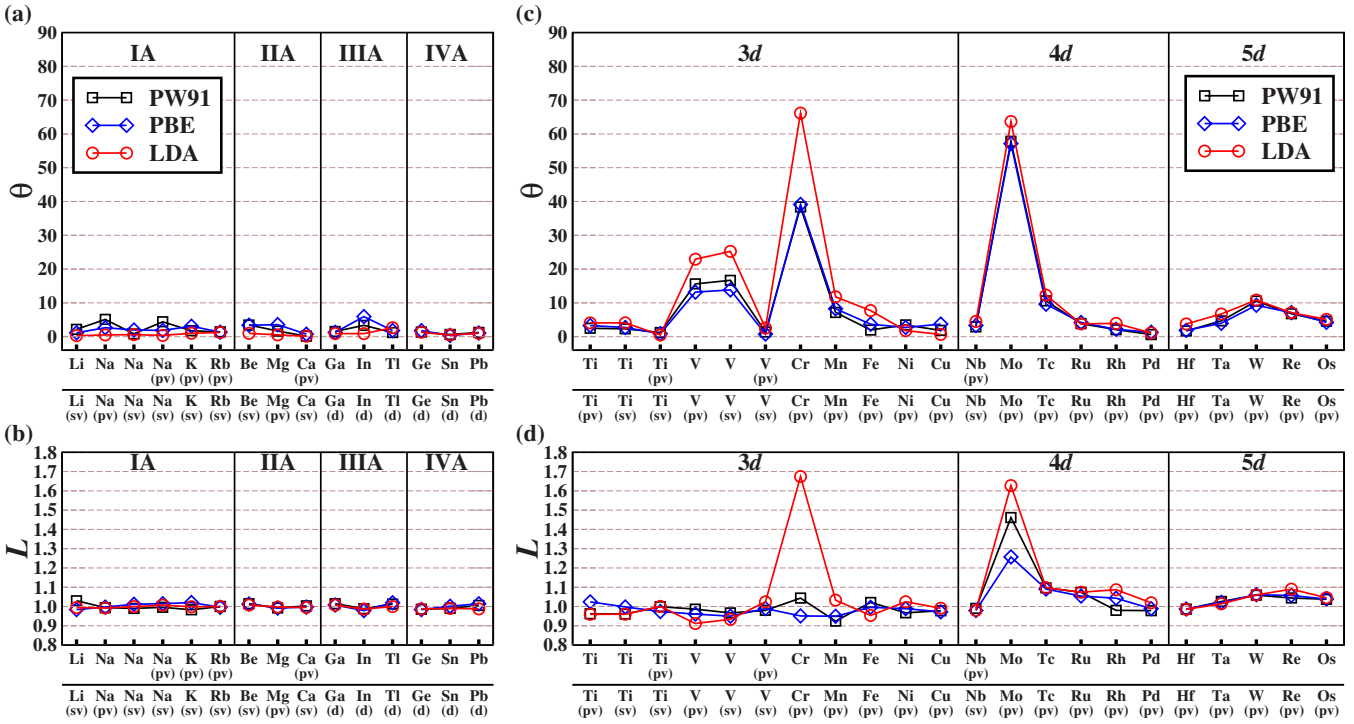

FIG. 4. (Color online) The correlation data between different PPs. The results of angle $\boldsymbol{\theta}$ and the relative amplitude $\boldsymbol{L}$ are summarized in (a) and (b) for Group A and (c) and (d) for Group B. The black square, blue diamond, and red circle represent PW91, PBE, and LDA, respectively.

values below 10° (except for Cr_{13}) and the relative amplitude $\boldsymbol{L}$ values in the range of 1.00 ± 0.10. When comparing the results from LDA and GGA, as red circles for $\vec{\mathfrak{D}}_M^{\mathrm{LDA}}/\vec{\mathfrak{D}}_M^{\mathrm{PW91}}$ and blue diamonds for $\vec{\mathfrak{D}}_M^{\mathrm{LDA}}/\vec{\mathfrak{D}}_M^{\mathrm{PBE}}$ in Fig. 2(c), values of angle $\boldsymbol{\theta}$ equal to or larger than 20° are observed for the Cr, Mn, Fe, Co, Ni, and Rh 13-atom clusters. Figure 2(d) shows that the value of the relative amplitude $\boldsymbol{L}$ of Mn_{13}, Fe_{13}, Ni_{13}, and Pd_{13} has a large deviation from unity.

TABLE I. The magnetic moment of nine isomer structures of IA–IVA metallic clusters, which are obtained from XC functionals of LDA (denoted as "L"), PW91 (denoted as "W"), and PBE (denoted as "P").

		ICO			FCC			DEC			BCC			HCP			BBP			TBP			GCL			CAG		
	Element	L	W	P	L	W	P	L	W	P	L	W	P	L	W	P	L	W	P	L	W	P	L	W	P	L	W	P
IA	Li(*sv*)	5	5	5	5	5	5	5	5	5	5	5	5	5	5	5	1	1	1	1	1	1	1	1	1	1	1	1
	Na(*sv*)	5	5	5	5	5	5	5	5	5	3	3	3	5	5	5	1	1	1	1	1	1	1	1	1	1	1	1
	K(*sv*)	5	5	5	1	1	1	5	5	5	1	1	1	5	5	5	1	1	1	1	1	1	1	1	1	1	1	1
	Rb(*sv*)	5	5	5	1	1	1	5	5	5	1	1	1	5	5	5	1	1	1	1	1	1	1	1	1	1	1	1
	Cs(*sv*)	5	5	5	1	1	1	1	1	1	3	3	3	1	1	1	1	1	1	1	1	0	1	1	1	1	1	0
IIA	Be(*sv*)	6	6	6	2	2	2	0	0	0	2	2	2	4	4	4	0	0	0	0	0	0	2	2	2	0	0	0
	Mg(*pv*)	6	6	6	4	4	4	6	6	6	0	2	2	2	2	2	0	0	0	0	0	0	0	0	0	2	2	2
	Ca(*sv*)	0	0	0	6	6	6	6	6	6	2	2	2	2	2	2	2	2	2	0	0	0	0	2	2	2	2	2
	Sr(*sv*)	0	0	0	6	6	6	4	4	4	0	0	0	2	2	2	2	2	2	0	0	0	0	2	2	2	2	2
	Ba(*sv*)	0	0	0	4	6	6	2	2	2	0	0	0	4	6	6	2	2	2	2	2	2	0	0	0	0	0	0
IIIA	Al	1	1	1	1	1	1	1	1	1	1	1	1	1	1	1	1	1	1	1	1	1	1	1	1	1	1	1
	Ga(*d*)	1	1	1	1	1	1	1	1	1	1	1	1	1	1	1	1	1	1	1	1	1	1	1	1	1	1	1
	In(*d*)	1	1	1	1	1	1	1	1	1	1	1	1	1	1	1	1	1	1	1	1	1	1	1	1	1	1	1
	Tl(*d*)	1	1	1	1	1	1	1	1	1	1	1	1	1	1	1	1	1	1	1	1	1	1	1	1	1	1	1
IVA	Ge(*d*)	0	0	0	2	2	2	2	2	2	0	0	0	2	2	2	0	0	0	0	0	0	0	0	0	0	0	0
	Sn(*d*)	0	0	0	2	2	2	2	2	2	0	0	0	2	2	2	0	0	0	0	0	0	0	0	0	0	0	0
	Pb(*d*)	0	0	0	0	0	0	0	0	0	0	0	0	2	2	2	0	0	0	2	2	2	0	0	0	2	2	2

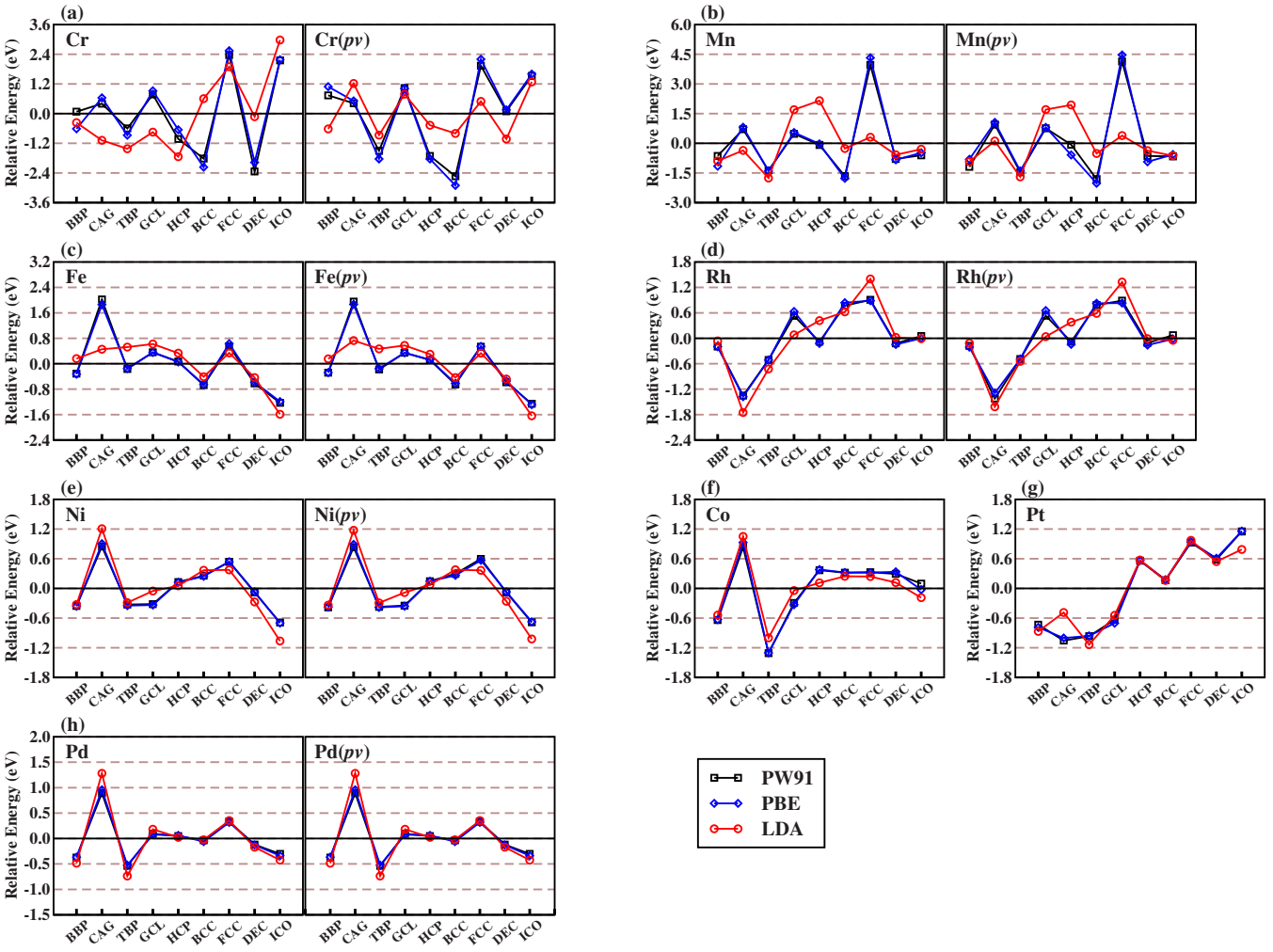

FIG. 5. (Color online) The relative energy plots of 13-atom metallic clusters for (a) Cr and Cr(*pv*); (b) Mn and Mn(*pv*); (c) Fe and Fe(*pv*); (d) Rh and Rh(*pv*); (e) Ni and Ni(*pv*); (f) Co; (g) Pt; (h) Pd and Pd(*pv*), which obtained from PW91 (black square), PBE (blue diamond), and LDA (red circle).

Specifically, for Cr_{13}, the left panel of Fig. 5(a) shows that the curves of relative energy (or displacement vectors) for LDA and GGA are significantly different. Furthermore, after considering the PP with the *p*-type semicore state, as shown in the right panel of Fig. 5(a), the discrepancy between LDA and GGA is still observed. Noticeably, in comparing the relative energy plots of Cr_{13} and $Cr_{13}(pv)$, the individual results obtained from either GGA or LDA exhibit a significant divergence. This discrepancy implies that the PP of Cr with the *p*-type semicore state is needed. However, it is unclear whether the deeper *s*-type semicore state is needed to obtain reliable and converging results.

For Mn_{13}, the angle $\boldsymbol{\theta}$ values obtained from $\vec{\mathfrak{D}}_{\mathrm{Mn}}^{\mathrm{LDA}}/\vec{\mathfrak{D}}_{\mathrm{Mn}}^{\mathrm{PW91}}$ and $\vec{\mathfrak{D}}_{\mathrm{Mn}}^{\mathrm{LDA}}/\vec{\mathfrak{D}}_{\mathrm{Mn}}^{\mathrm{PBE}}$ are about 70°. In addition, the relative amplitude of $\vec{\mathfrak{D}}_{\mathrm{Mn}}^{\mathrm{LDA}}/\vec{\mathfrak{D}}_{\mathrm{Mn}}^{\mathrm{PW91}}$ is 0.73 and that of $\vec{\mathfrak{D}}_{\mathrm{Mn}}^{\mathrm{LDA}}/\vec{\mathfrak{D}}_{\mathrm{Mn}}^{\mathrm{PBE}}$ is 0.67. These correlation data can be compared with the relative energy profiles, as shown in the left panel of Fig. 5(b). The discrepancy between LDA and GGA results in a larger angle $\boldsymbol{\theta}$, and the relative amplitude $\boldsymbol{L}$ significantly deviates from unity. For $Mn_{13}(pv)$, in the right panel of Fig. 5(b), it is clear that a *p*-type semicore state does not improve the consistency between LDA and GGA. Similar to Mn_{13}, for the displacement vectors of Fe_{13}, Rh_{13}, and Ni_{13}, shown in Figs. 5(c)–5(e), in spite of treating *p*-type semicore state as valence electrons, the relative energies obtained from LDA still deviate from those of GGA. With respect to Co_{13}, as shown in Fig. 5(f), large energy deviations between LDA and GGA are observed for the TBP, GCL, HCP, DEC, and ICO isomers, with an angle $\boldsymbol{\theta}$ of about 20°. Additionally, for Pt_{13}, shown in Fig. 5(g), an obvious discrepancy in the CAG and ICO isomers is observed. For the correlation data of Pd_{13}, the angles $\boldsymbol{\theta}$ values are all less than 5°. However, the values of the relative amplitude are greater than 1.3 for $\vec{\mathfrak{D}}_{\mathrm{Pd}}^{\mathrm{LDA}}/\vec{\mathfrak{D}}_{\mathrm{Pd}}^{\mathrm{GGA}}$. As can be seen in the left panel of Fig. 5(h), LDA produces the same energy ordering as GGA. However, when comparing the absolute value of the relative energy, LDA obtained larger values than GGA for most isomers, except for the HCP and BCC structures. For a larger deviation in the relative energy, one might expect that the $\boldsymbol{L}$ value would deviate significantly from unity. Nevertheless, this is not the case for some elements. For instance, the LDA results for Cr_{13} are not consistent with the GGA results, as shown in Fig. 5(a), but the $\boldsymbol{L}$ value is 0.97, which is obviously closer to unity than the result for Pd_{13}. This implies that a value of $\boldsymbol{L}$ close to

unity does not necessarily indicate a good correlation between two displacement vectors. A detailed study of the relative amplitude $\boldsymbol{L}$ will be presented and the relative deviation (the difference between two displacement vectors) will be introduced and discussed in Sec. III C.

As commonly believed, in most cases, the consistency of the results between PW91 and PBE is better than that between GGA and LDA. We have also observed this trend in the correlation analyses. Furthermore, the consistency of the three XC functionals in the 4*d* and 5*d* series of transition metals is better than that in 3*d*. For the Cr, Mn, Fe, Co, Ni, and Rh clusters, the usage of the LDA and GGA functionals produces different displacement vectors. However, it is believed that the results of GGA should be more correct.

2. Pseudopotential dependence

Correlation analyses for 3*d*, 4*d*, and 5*d* transition metals, with and without considering the semicore states, are displayed in Figs. 4(c) and 4(d). The PPs with semicore states from the VASP database include 18 elements, which are Ti, V, Cr, Mn, Fe, Ni, Cu, Nb, Mo, Tc, Ru, Rh, Pd, Hf, Ta, W, Re, and Os. For a comparison between different PPs, there exist three combinations as follows: (i) $\vec{\mathfrak{D}}_{M}^{\mathrm{XC}}/\vec{\mathfrak{D}}_{M(pv)}^{\mathrm{XC}}$ for M=Cr, Mn, Fe, Ni, Cu, Mo, Tc, Ru, Rh, Pd, Hf, Ta, W, Re, and Os, (ii) $\vec{\mathfrak{D}}_{M(pv)}^{\mathrm{XC}}/\vec{\mathfrak{D}}_{M(sv)}^{\mathrm{XC}}$ for M=Nb, and (iii) $\vec{\mathfrak{D}}_{M}^{\mathrm{XC}}/\vec{\mathfrak{D}}_{M(pv)}^{\mathrm{XC}}$, $\vec{\mathfrak{D}}_{M}^{\mathrm{XC}}/\vec{\mathfrak{D}}_{M(sv)}^{\mathrm{XC}}$, and $\vec{\mathfrak{D}}_{M(pv)}^{\mathrm{XC}}/\vec{\mathfrak{D}}_{M(sv)}^{\mathrm{XC}}$ for M=Ti and V.

Regarding the 3*d* series shown in Fig. 4(c), values of the angles $\boldsymbol{\theta}$ larger than 10° are observed for the four cases of $\vec{\mathfrak{D}}_{\mathrm{V}}^{\mathrm{XC}}/\vec{\mathfrak{D}}_{\mathrm{V}(pv)}^{\mathrm{XC}}$, $\vec{\mathfrak{D}}_{\mathrm{V}}^{\mathrm{XC}}/\vec{\mathfrak{D}}_{\mathrm{V}(sv)}^{\mathrm{XC}}$, $\vec{\mathfrak{D}}_{\mathrm{Cr}}^{\mathrm{XC}}/\vec{\mathfrak{D}}_{\mathrm{Cr}(pv)}^{\mathrm{XC}}$, and $\vec{\mathfrak{D}}_{\mathrm{Mn}}^{\mathrm{LDA}}/\vec{\mathfrak{D}}_{\mathrm{Mn}(pv)}^{\mathrm{LDA}}$. As shown in the relative amplitude plot in Fig. 4(d), most of the $\boldsymbol{L}$ values approach unity (the ranges are from 1.04 to 0.91), apart from $\vec{\mathfrak{D}}_{\mathrm{Cr}}^{\mathrm{LDA}}/\vec{\mathfrak{D}}_{\mathrm{Cr}(pv)}^{\mathrm{LDA}}$ whose value is 1.67. For V_{13}, the valence configurations of V, V(*pv*), and V(*sv*) are $3d^4 4s^1$, $3p^6 3d^4 4s^1$, and $3s^2 3p^6 3d^4 4s^1$, respectively. Figures 4(c) and 4(d) show that $\vec{\mathfrak{D}}_{\mathrm{V}(pv)}^{\mathrm{XC}}$ and $\vec{\mathfrak{D}}_{\mathrm{V}(sv)}^{\mathrm{XC}}$ have a great consistency for the three XC functionals with angles $\boldsymbol{\theta}$ values less than 3° and $\boldsymbol{L}$ values of approximately 1.00 ± 0.02. However, for $\vec{\mathfrak{D}}_{\mathrm{V}}^{\mathrm{XC}}/\vec{\mathfrak{D}}_{\mathrm{V}(pv)}^{\mathrm{XC}}$ and $\vec{\mathfrak{D}}_{\mathrm{V}}^{\mathrm{XC}}/\vec{\mathfrak{D}}_{\mathrm{V}(sv)}^{\mathrm{XC}}$, the consistency is worse, where the angle $\boldsymbol{\theta}$ values are between 13° and 25°. Comparing these correlation data with the displacement vectors shown in Fig. 6(a), it is obvious that the relative energies of V(*pv*) and V(*sv*) exhibit very high similarity for the three XC functionals. Therefore, these results reveal that the semicore states are very important for V_{13} and that the usage of the *p*-type semicore state is sufficient to provide a reliable result. Moreover, the consistency between LDA and GGA is also remarkably improved after using the deeper semicore PPs.

For Cr_{13}, shown in Fig. 4(c), the angles $\boldsymbol{\theta}$ values of $\vec{\mathfrak{D}}_{\mathrm{Cr}}^{\mathrm{LDA}}/\vec{\mathfrak{D}}_{\mathrm{Cr}(pv)}^{\mathrm{LDA}}$ and $\vec{\mathfrak{D}}_{\mathrm{Cr}}^{\mathrm{GGA}}/\vec{\mathfrak{D}}_{\mathrm{Cr}(pv)}^{\mathrm{GGA}}$ are 66° and 39°, respectively. In Fig. 5(a), it is shown that the relative energy curves for Cr and Cr(*pv*) are significantly different. This discrepancy indicates that the PP with the *p*-type semicore state is needed. However, as was mentioned earlier (in Sec. III B 1), inconsistency between LDA and GGA is still observed when including the *p*-type semicore state. For Mn_{13}, the angle $\boldsymbol{\theta}$ values of $\vec{\mathfrak{D}}_{\mathrm{Mn}}^{\mathrm{XC}}/\vec{\mathfrak{D}}_{\mathrm{Mn}(pv)}^{\mathrm{XC}}$ range from 7° to 12°. As is evident from their relative energy profiles, shown in Fig. 5(b), we conclude that the usage of semicore PPs can be neglected since only little improvement is obtained.

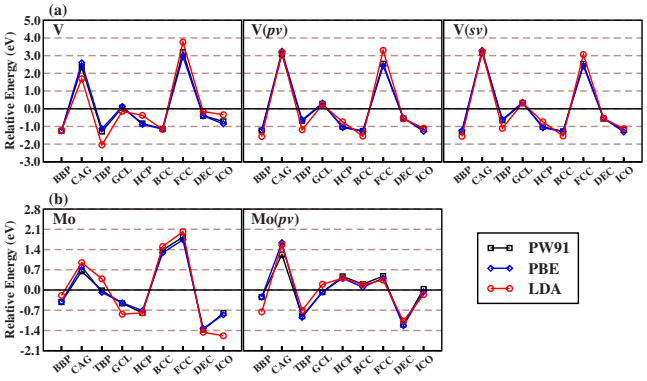

FIG. 6. (Color online) The relative energy plots of 13-atom metallic clusters of (a) V, V(*pv*), and V(*sv*); (b) Mo and Mo(*pv*), which obtained from PW91 (black square), PBE (blue diamond), and LDA (red circle).

When considering 4*d* series, the correlation data in Fig. 4(c) illustrates that the angle $\boldsymbol{\theta}$ values of $\vec{\mathfrak{D}}_{\mathrm{Mo}}^{\mathrm{GGA}}/\vec{\mathfrak{D}}_{\mathrm{Mo}(pv)}^{\mathrm{GGA}}$ and $\vec{\mathfrak{D}}_{\mathrm{Mo}}^{\mathrm{LDA}}/\vec{\mathfrak{D}}_{\mathrm{Mo}(pv)}^{\mathrm{LDA}}$ are the poorest at 58° and 64°, respectively. Likewise, large $\boldsymbol{L}$ values of Mo_{13} are found, with 1.3 for PBE, 1.5 for PW91, and 1.6 for LDA, as shown in Fig. 4(d). Comparing the displacement vectors of Mo and Mo(*pv*) in Fig. 6(b), the relative energies of the nine isomers are significantly different. As a consequence, the consideration of PPs with the *p*-type semicore state is definitely required when calculating Mo metallic clusters. However, it is still unclear whether a deeper *s*-type semicore PP is needed to obtain a converging result. For the correlation data of the 5*d* series, presented in Figs. 4(c) and 4(d), all of the angle $\boldsymbol{\theta}$ values are less than 11° and the relative amplitudes are in the range from 0.99 to 1.09. This implies that the PPs without semicore states are reliable for the study of 5*d* transition metallic clusters.

The magnetic moments of 13-atom metallic clusters for 3*d*, 4*d*, and 5*d* group elements are given in Table II. It is found that all the magnetic moment obtained by using PW91 and PBE are exactly the same. For the results obtained by LDA and GGA, 4*d* and 5*d* groups are more consistent than that by 3*d* group transition metals. However, the magnetic moment of Ir(TBP) cluster obtained by LDA and GGA differ by $10\mu_B$. For 3*d* group, the middle transition metals, i.e., Cr(BCC), Mn(CBP), Fe(BBP, CAG, and FCC), and Co(ICO), the LDA magnetic moments are different from GGA magnetic moments for more than $8\mu_B$. We believe that GGA should give more accurate results than LDA. To summarize the studies of the dependence on PPs in Group B, the usage of the semicore state is significant for V_{13}, Cr_{13}, and Mo_{13}, while the dependence on PPs is smaller for the other elements.

C. Relative deviation

As mentioned in Sec. III B 1, when examining the relative amplitude profiles in Fig. 2(d), it is difficult to verify the consistency between LDA and GGA for Cr_{13}. This is due to

TABLE II. The magnetic moment of nine isomer structures of metallic clusters in 3*d*, 4*d*, and 5*d* serials, which are obtained from XC functionals of LDA (denoted as L), PW91 (denoted as W), and PBE (denoted as P).

		ICO			FCC			DEC			BCC			HCP			BBP			TBP			GCL			CAG		
	Element	L	W	P	L	W	P	L	W	P	L	W	P	L	W	P	L	W	P	L	W	P	L	W	P	L	W	P
3*d*	Sc(*sv*)	19	19	19	3	3	3	11	11	11	7	9	9	1	3	3	7	9	9	5	5	5	5	7	7	3	7	7
	Ti(*sv*)	6	6	6	10	10	10	2	2	2	6	6	6	2	2	2	2	2	2	2	4	4	4	4	4	4	4	4
	V(*sv*)	7	7	7	7	13	13	1	1	1	1	1	1	7	7	7	1	1	1	1	3	3	3	3	3	1	1	1
	Cr(*pv*)	20	20	20	2	2	2	2	2	2	10	20	20	8	8	8	0	0	0	2	2	2	0	0	0	2	2	2
	Mn(*pv*)	33	33	33	5	11	11	17	17	17	15	13	13	35	39	39	9	3	3	5	23	23	27	33	33	7	7	7
	Fe(*pv*)	34	34	34	32	40	40	36	38	38	36	38	38	36	38	38	32	40	40	38	40	40	38	40	40	16	40	40
	Co	21	31	31	21	27	27	21	23	23	21	27	27	21	23	23	23	25	25	27	27	27	25	25	25	23	25	25
	Ni(*pv*)	8	8	8	6	6	6	8	8	8	10	10	10	6	8	8	10	10	10	8	12	12	12	12	12	10	10	10
	Cu(*pv*)	5	5	5	1	1	1	1	1	1	1	1	1	3	3	3	1	1	1	1	1	1	1	1	1	1	1	1
4*d*	Y(*sv*)	13	19	19	3	3	3	11	11	11	3	3	3	3	3	3	7	7	7	5	5	5	1	5	5	3	3	3
	Zr(*sv*)	6	6	6	0	0	0	2	2	2	2	2	2	2	2	2	2	2	2	0	0	0	2	4	4	0	0	0
	Nb(*sv*)	3	7	7	1	1	1	1	1	1	1	1	1	1	3	3	1	1	1	1	1	1	1	1	1	1	1	1
	Mo(*sv*)	2	2	2	2	2	2	2	2	2	2	2	2	2	2	2	0	0	0	0	0	0	2	2	2	0	0	0
	Tc(*pv*)	13	13	13	5	5	5	6	6	6	5	5	5	1	1	1	3	3	3	1	1	1	1	1	1	1	1	1
	Ru(*pv*)	12	12	12	8	18	18	8	8	8	6	8	8	2	4	4	4	6	6	2	8	8	4	4	4	2	2	2
	Rh(*pv*)	15	17	17	19	19	19	11	17	17	5	5	5	15	19	19	15	17	17	11	11	11	3	5	5	5	9	9
	Pd(*pv*)	8	8	8	6	6	6	6	8	8	4	4	4	6	6	6	4	4	4	2	6	6	6	6	6	4	4	4
	Ag	5	5	5	1	1	1	1	1	1	1	1	1	3	3	3	1	1	1	1	1	1	1	1	1	1	1	1
5*d*	La	3	3	3	3	3	3	3	3	3	3	3	3	1	3	3	1	1	1	1	1	1	1	1	1	1	1	1
	Hf(*pv*)	6	6	6	4	4	4	2	2	2	2	2	2	2	2	2	2	2	2	2	2	2	2	2	2	0	0	0
	Ta(*pv*)	3	7	7	3	7	7	3	3	3	1	1	1	1	3	3	1	1	1	1	1	1	1	1	1	3	3	3
	W(*pv*)	4	4	4	2	2	2	2	2	2	0	0	0	2	6	6	4	4	4	0	0	0	2	2	2	0	0	0
	Re(*pv*)	13	13	13	5	5	5	3	7	7	5	7	7	1	1	1	3	9	9	3	5	5	1	1	1	1	1	1
	Os(*pv*)	2	2	2	8	8	8	4	8	8	3	4	4	2	2	2	0	4	4	4	4	4	6	6	6	4	4	4
	Ir	1	1	1	19	19	19	5	5	5	7	7	7	5	5	5	3	3	3	1	11	11	5	7	7	3	3	3
	Pt	2	2	2	6	6	6	4	4	4	0	2	2	6	6	6	4	4	4	0	0	0	2	2	2	2	2	2
	Au	5	5	5	1	1	1	1	1	1	1	1	1	1	3	3	1	1	1	1	1	1	1	1	1	1	1	1

the compensation between the components (i.e., the individual isomer energy) of a displacement vector. For the relative energy profile of Cr_{13} in the left panel of Fig. 5(a), LDA obtained higher energies (in absolute value) than GGA for the CAG, TBP, GCL, HCP, and ICO structures, but had lower energies (in absolute value) for the BCC, FCC, and DEC structures. In contrast, for Pd_{13}, shown in Fig. 5(i), the absolute values of relative energy from LDA are larger than those of GGA for most isomer structures, except for HCP and BCC. Figures 7(a) and 7(b) show the geometric relation between the two displacement vectors $\vec{\mathfrak{D}}_M^{\mathrm{LDA}}$ and $\vec{\mathfrak{D}}_M^{\mathrm{PW91}}$ of Cr_{13} and Pd_{13}, respectively. As seen from Fig. 7(a) for Cr_{13}, the $\boldsymbol{L}$ ($|\vec{\mathfrak{D}}_{\mathrm{Cr}}^{\mathrm{LDA}}|/|\vec{\mathfrak{D}}_{\mathrm{Cr}}^{\mathrm{PW91}}|$) value and $\boldsymbol{\theta}$ value are 0.97° and 55.2°, and from Fig. 7(b) for Pd_{13}, the $\boldsymbol{L}$ value and $\boldsymbol{\theta}$ value are 1.38° and 4.8°, respectively. Here, for Cr_{13}, $|\vec{\mathfrak{D}}_{\mathrm{Cr}}^{\mathrm{LDA}}|$ approaches $|\vec{\mathfrak{D}}_{\mathrm{Cr}}^{\mathrm{PW91}}|$, and for Pd_{13}, $|\vec{\mathfrak{D}}_{\mathrm{Pd}}^{\mathrm{LDA}}|$ is 38% larger than $|\vec{\mathfrak{D}}_{\mathrm{Pd}}^{\mathrm{PW91}}|$. From the illustration presented here, one can see that, for the correlation analysis, $\boldsymbol{L}$ values closer to unity (as in the Cr_{13} case) do not imply a better consistency than values that deviate largely from unity (as in the Pd_{13} case). Alternatively, one can use the vector difference between two displacement vectors, which will be helpful in the correlation analysis. Here we define the relative deviation (RD) between the displacement vectors $\vec{\mathfrak{D}}_M^A$ and $\vec{\mathfrak{D}}_M^B$ as follows:

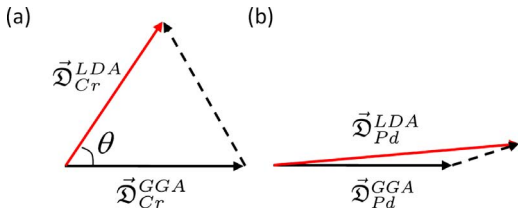

FIG. 7. (Color online) The schematic of two displacement vectors of (a) Cr, where $\vec{\mathfrak{D}}_{\mathrm{Cr}}^{\mathrm{LDA}}/\vec{\mathfrak{D}}_{\mathrm{Cr}}^{\mathrm{GGA}}=0.97$ and $\boldsymbol{\theta}=55.2°$; (b) Pd, where $\vec{\mathfrak{D}}_{\mathrm{Pd}}^{\mathrm{LDA}}/\vec{\mathfrak{D}}_{\mathrm{Pd}}^{\mathrm{GGA}}=1.38$ and $\boldsymbol{\theta}=4.8°$.

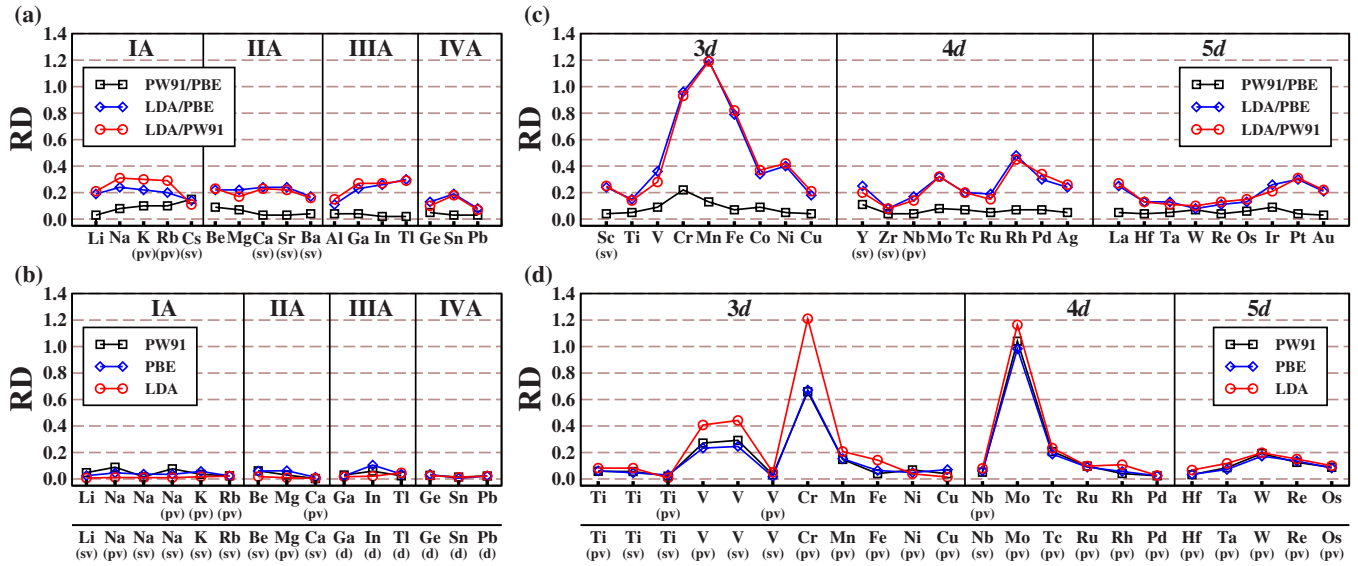

FIG. 8. (Color online) The relative deviation between (a) different XC functionals for Group A; (b) different PPs for Group A; (c) different XC functionals for Group B; and (d) different PPs for Group B.

$$\mathrm{RD} = \frac{|\vec{\mathfrak{D}}_a^A - \vec{\mathfrak{D}}_b^B|}{\sqrt{|\vec{\mathfrak{D}}_a^A||\vec{\mathfrak{D}}_b^B|}} = \sqrt{\frac{|\vec{\mathfrak{D}}_a^A|^2 + |\vec{\mathfrak{D}}_b^B|^2 - 2|\vec{\mathfrak{D}}_a^A||\vec{\mathfrak{D}}_b^B|\cos\boldsymbol{\theta}}{|\vec{\mathfrak{D}}_a^A||\vec{\mathfrak{D}}_b^B|}}. \tag{3}$$

It is clear that the RD includes the information of $\boldsymbol{L}$ and $\cos(\boldsymbol{\theta})$. The relative deviation profiles of different XC functionals and different PPs are presented in Fig. 8. As can be seen in Fig. 8(a), the RD values of $\vec{\mathfrak{D}}_{\mathrm{Cr}}^{\mathrm{LDA}}$ and $\vec{\mathfrak{D}}_{\mathrm{Cr}}^{\mathrm{GGA}}$ are roughly 0.93, while the RD values of $\vec{\mathfrak{D}}_{\mathrm{Pd}}^{\mathrm{LDA}}$ and $\vec{\mathfrak{D}}_{\mathrm{Pd}}^{\mathrm{GGA}}$ are 0.34 and 0.30, respectively. Therefore, one can conclude that the consistency between LDA and GGA for Pd_{13} is better than that for Cr_{13}, as is evident from Figs. 5(a) and 5(h).

As discussed above, among the three correlation parameters, $\boldsymbol{\theta}$, $\boldsymbol{L}$, and RD, our studies show that the angle $\boldsymbol{\theta}$ is more sensitive in judging whether a good correlation exists. When the angle $\boldsymbol{\theta}$ value is small, it will give a good correlation, even if RD is large or $\boldsymbol{L}$ greatly deviates from unity. On the other hand, a large value of RD does not imply a poor correlation if $\boldsymbol{\theta}$ is small, for example, as in the Pd case shown in Fig. 7(b). Additionally, for $\boldsymbol{L}$ values close to unity, a good correlation is not implied if $\boldsymbol{\theta}$ is large, for example, as in the Cr case shown in Fig. 7(a). To conclude, a good correlation between two displacement vectors will be obtained only when (i) the angle $\boldsymbol{\theta}$ value is small (less than 5°); (ii) $\boldsymbol{L}$ is close to unity; and (iii) RD approaches zero.

IV. SUMMARY

We have presented a systematic study of the relative isomer energies of 13-atom clusters using various XC functionals (LDA, PW91, and PBE) and PPs for 44 metallic elements throughout the periodic table, including IA, IIA, IIIA, and IVA (Group A) and 3*d*, 4*d*, and 5*d* (Group B) elements. Five high-symmetry three-dimensional and four low-symmetry layer-type isomer structures were considered for each element. To provide a quantitative analysis, we defined the displacement vectors with dependence on XC functionals and PPs. The correlation analyses [see Eqs. (1) and (2)] between displacement vectors are then introduced to provide quantitative comparisons of the calculated results obtained from different XC functionals and PPs. Regarding whether the lowest-energy structure of nine selected isomer corresponds to the actual global minimum, we have found that for Li, In, Y, Zr, Tc, Ru, Rh,h Re, Os, and Ir, the lowest energy structures of 13-atom clusters among nine isomers studied in this work correspond to the actual global minimum found by a recent exhaust work.[12]

From our results, the larger deviations are obtained for three elements, $\mathrm{Cr}(3d^5 4s^1)$, $\mathrm{Mn}(3d^5 4s^2)$, and $\mathrm{Mo}(4d^5 5s^1)$. The common feature of a half filled of *d* and/or *s* orbital leads to exceptional properties like the occurrence of dimmer growth route,[31] inconstant magnetic configurations and magnetic moments[32] as a function of cluster sizes as well as the existence of the nearly degenerate states,[33,34] to name a few. It is well known that the physical properties of these systems, e.g., ionization potential, bond length, binding energy, and magnetic moment, depend strongly on the particular type of the exchange-correlation energy functional employed in the DFT calculations.[35] The present results, obtained through a systematic study over the transition elements and designed quantitative measurement, demonstrate clearly the inconsistency in different DFT calculations for these systems, as compared to those made of the rest of the transition elements.

For Group A, we found that the relative isomer energies obtained using different XC functionals (LDA, PW91, and PBE) exhibit a great consistency. Furthermore, our studies showed that the usage of PPs with the semicore state is unnecessary. For Group B, the correlation analyses indicated

that the consistency of the three XC functionals for 5*d* is better than that of 4*d*, followed by 3*d*. The consistency of the results between two GGA functionals was shown to be better than that between LDA and GGA, as commonly believed. For the Cr, Mn, Fe, Co, Ni, and Rh clusters, the relative isomer energies predicted by the LDA and GGA functionals are quite different. However, it is believed that the results of GGA are more correct. Moreover, our results indicate that inclusion of the semicore states in the PPs is not necessary for most elements in Group B, while for studies including V, Cr, and/or Mo elements, the usage of deeper semicore states in the PPs is inevitable.

ACKNOWLEDGMENTS

This work was supported in part by the National Science Council of Taiwan under Grant No. 96-2628-M001-006-MY3. We also acknowledge the National Center for Theoretical Sciences (NCTS) and computing resources from the National Center for High-Performance Computing (NCHC) in Taiwan.

*cmw@phys.sinica.edu.tw

[1] F. Baletto and R. Ferrando, Rev. Mod. Phys. **77**, 371 (2005).
[2] J. D. Aiken and R. G. Finke, J. Mol. Catal. A: Chem. **145**, 1 (1999).
[3] G. Schmid, M. Bäumle, M. Geerkens, I. Heim, C. Osemann, and T. Sawitowski, Chem. Soc. Rev. **28**, 179 (1999).
[4] *Quantum Phenomena in Clusters and Nanostructures*, edited by S. N. Khanna and A. W. Castleman (Springer-Verlag, Heidelberg, 2003).
[5] Robert F. Service, Science **271**, 920 (1996).
[6] M. Sakurai, K. Watanabe, K. Sumiyama, and K. Suzuki, J. Chem. Phys. **111**, 235 (1999).
[7] C. M. Chang and M. Y. Chou, Phys. Rev. Lett. **93**, 133401 (2004).
[8] T. Futschek, J. Hafner, and M. Marsman, J. Phys.: Condens. Matter **18**, 9703 (2006).
[9] J. Rogan, G. Garcia, C. Loyola, W. Orellana, R. Ramirez, and M. Kiwi, J. Chem. Phys. **125**, 214708 (2006).
[10] R. C. Longo and L. J. Gallego, Phys. Rev. B **74**, 193409 (2006).
[11] L.-L. Wang and D. D. Johnson, Phys. Rev. B **75**, 235405 (2007).
[12] Y. Sun, M. Zhang, and R. Fournier, Phys. Rev. B **77**, 075435 (2008).
[13] F. Aguilera-Granja, A. Garcia-Fuente, and A. Vega, Phys. Rev. B **78**, 134425 (2008).
[14] H. Häkkinen, M. Moseler, and U. Landman, Phys. Rev. Lett. **89**, 033401 (2002).
[15] P. Hohenberg and W. Kohn, Phys. Rev. **136**, B864 (1964); W. Kohn and L. J. Sham, Phys. Rev. **140**, 1133 (1965).
[16] H. Häkkinen and U. Landman, Phys. Rev. B **62**, R2287 (2000); H. Häkkinen, B. Yoon, U. Landman, X. Li, H.-J. Zhai, and L.-S. Wang, J. Phys. Chem. A **107**, 6168 (2003).
[17] J. Oviedo and R. E. Palmer, J. Chem. Phys. **117**, 9548 (2002).
[18] V. Kumar and Y. Kawazoe, Phys. Rev. B **66**, 144413 (2002).
[19] V. Kumar and Y. Kawazoe, Eur. Phys. J. D **24**, 81 (2003).
[20] Y.-C. Bae, H. Osanai, V. Kumar, and Y. Kawazoe, Phys. Rev. B **70**, 195413 (2004).
[21] L.-L. Wang and D. D. Johnson, J. Phys. Chem. B **109**, 23113 (2005).
[22] J. P. Perdew and A. Zunger, Phys. Rev. B **23**, 5048 (1981).
[23] J. P. Perdew, J. A. Chevary, S. H. Vosko, K. A. Jackson, M. R. Pederson, D. J. Singh, and C. Fiolhais, Phys. Rev. B **46**, 6671 (1992).
[24] J. P. Perdew, K. Burke, and M. Ernzerhof, Phys. Rev. Lett. **77**, 3865 (1996).
[25] D. Vanderbilt, Phys. Rev. B **41**, 7892 (1990).
[26] G. Kresse and J. Furthmuller, Phys. Rev. B **54**, 11169 (1996).
[27] P. E. Blöchl, Phys. Rev. B **50**, 17953 (1994).
[28] Y. C. Bae, V. Kumar, H. Osanai, and Y. Kawazoe, Phys. Rev. B **72**, 125427 (2005).
[29] V. Kumar and Y. Kawazoe, Phys. Rev. B **65**, 125403 (2002).
[30] C. R. Hsing, C. M. Wei, N. D. Drummond, and R. J. Needs, Phys. Rev. B **79**, 245401 (2009).
[31] H. Cheng and L. S. Wang, Phys. Rev. Lett. **77**, 51 (1996).
[32] F. W. Payne, W. Jiang, and L. A. Bloomfield, Phys. Rev. Lett. **97**, 193401 (2006).
[33] P. Bobadova-Parvanova, K. A. Jackson, S. Srinivas, and M. Horoi, Phys. Rev. A **67**, 061202(R) (2003).
[34] S. N. Khanna, B. K. Rao, P. Jena, and M. Knickelbein, Chem. Phys. Lett. **378**, 374 (2003).
[35] S. K. Nayak and P. Jena, Chem. Phys. Lett. **289**, 473 (1998).